Monthly Notices of the ROYAL ASTRONOMICAL SOCIETY

MNRAS **537,** 3499–3510 (2025) https://doi.org/10.1093/mnras/staf223
Advance Access publication 2025 February 6

2D light distributions of dwarf galaxies – key tests of the implementation of physical processes in simulations

A. E. Watkins [1]★ G. Martin [2] S. Kaviraj [1] C. Collins,[3] Y. Dubois,[4] K. Kraljic,[5] C. Pichon[4,6,7] and S. K. Yi[8]

[1]*Centre for Astrophysics Research, University of Hertfordshire, College Lane, Hatfield AL10 9AB, UK*
[2]*School of Physics and Astronomy, University of Nottingham, University Park, Nottingham NG7 2RD, UK*
[3]*Astrophysics Research Institute, Liverpool John Moores University, IC2 Building, Liverpool Science Park, 146 Brownlow Hill, Liverpool L3 5RF, UK*
[4]*Institut d'Astrophysique de Paris, Sorbonne Université, CNRS, UMR 7095, 98 bis Boulevard Arago, F-75014 Paris, France*
[5]*Observatoire Astronomique de Strasbourg, Université de Strasbourg, CNRS, UMR 7550, , F-67000 Strasbourg,, France.*
[6]*Université Paris-Saclay, CNRS, CEA, Institut de physique théorique, Gif-sur-Yvette, 91191, France.*
[7]*Kyung Hee University, Dept. of Astronomy & Space Science,Yongin-shi, Gyeonggi-do 17104,Republic of Korea.*
[8]*Department of Astronomy and Yonsei University Observatory, Yonsei University, Seoul 03722, Korea*

Accepted 2025 February 3. Received 2025 February 3; in original form 2024 November 18

ABSTRACT

Cosmological simulations provide much of the theoretical framework within which we interpret extragalactic observations. However, even if a given simulation reproduces the integrated properties of galaxies well, it may not reproduce the detailed structures of individual galaxies. Comparisons between the 2D light distributions of simulated and observed galaxies – particularly in the dwarf regime, where key processes like tidal perturbations and baryonic feedback most strongly influence galaxy structure – thus provide an additional valuable test of the simulation's efficacy. We compare scaling relations derived from mock observations of simulated galaxies, drawn from the two largest haloes in the high-resolution NEWHORIZON cosmological simulation, with galaxies in the Fornax Cluster. While Fornax is significantly more massive than either group, it is the lowest mass cluster in the local Universe and contains a well-studied population of spatially resolved dwarfs, hence serves as a useful benchmark. Per unit stellar mass, NEWHORIZON dwarfs are systematically larger in half-light radius, much fainter in surface brightness, and bluer in colour than their Fornax counterparts, albeit with similar light profile shapes. We discuss potential reasons for these discrepancies, including environmental effects, baryonic feedback, resolution, or couplings of these factors. As observations of dwarfs outside of the local Universe become more plentiful through ongoing or upcoming surveys such as *Euclid* and Legacy Survey of Space and Time, 2D comparisons such as these, where properties are measured in the same way across both simulations and observations, can place strong constraints on processes that alter the spatial distribution of baryons in galaxies.

Key words: galaxies: clusters: general – galaxies: clusters: individual: Fornax – galaxies: dwarf – galaxies: evolution – galaxies: fundamental parameters – galaxies: structure.

1 INTRODUCTION

The distribution of baryons within galaxies is the result of a long and complex interplay between many internal and external forces. For example, once cold gas forms into stars, the most massive of those stars eject energy and metals back into the gas during their lifespans (through stellar winds) and in their explosive death knells (e.g. Capriotti & Kozminski 2001; Oppenheimer & Davé 2006; Hopkins, Quataert & Murray 2012; Dale et al. 2014; Kobayashi, Karakas & Lugaro 2020), altering the means by which subsequent stellar populations can form. Likewise, collisions with other galaxies can rearrange the stellar or dark matter phase-space distributions of the involved systems (e.g. Toomre & Toomre 1972; Moore, Lake & Katz 1998; Mastropietro et al. 2005; Binney & Tremaine 2008; Méndez-Abreu et al. 2012; Eliche-Moral et al. 2018; Martin et al. 2018), permanently altering the galaxies' subsequent dynamical evolution.

Tracking the relative influences of these disparate phenomena on any individual galaxy's evolution is difficult in the real Universe, and so we rely on large-scale simulations to construct narratives matching observations (e.g. Springel et al. 2005, 2018; Dubois et al. 2014; Vogelsberger et al. 2014; Schaye et al. 2015; Kaviraj et al. 2017). Necessarily, however, these simulations are constructed using physical assumptions derived from observations, so the two regimes – theoretical and observational – inform and build off of each other. While the origin and evolution of large-scale structure, such as galaxy clustering, is well constrained in our current cosmological paradigm of Λ cold dark matter (ΛCDM; e.g. Guo et al. 2011), fully realizing the detailed small-scale evolution of galaxies remains a work in progress.

★ E-mail: a.emery.watkins@gmail.com

Proposed resolutions to some small-scale problems, such as the 'missing satellites' problem (Klypin et al. 1999; Moore et al. 1999) or the 'too big to fail' problem (Boylan-Kolchin, Bullock & Kaplinghat 2011), rely on a confluence of factors, including the relationship between baryonic and dark matter, the completeness limits of existing all-sky surveys, and the impact of environment or baryonic feedback on gas retention and star formation (e.g. Guo et al. 2011; Sawala et al. 2016; Kim, Peter & Hargis 2018; Jackson et al. 2021b). The latter factor is critical, as without some kind of preventative feedback, stars condense in the centres of massive galaxies and in low-mass galaxies far too quickly (e.g. White & Rees 1978; Cole 1991; White & Frenk 1991; Beckmann et al. 2017).

The choice of feedback model is not a trivial one, however, as different models can produce degenerate results (e.g. Wright et al. 2024, and references therein). Some degeneracy is, of course, expected: the broad impact of feedback is to push against runaway gravitational collapse, and so serves as a means for systems to self-regulate. However, in modern simulations, the feedback is often calibrated to reproduce a narrow set of fundamental scaling relations, such as the stellar mass function (e.g. Dayal et al. 2014; McCarthy et al. 2017) or the cosmic star formation history (e.g. Schaye et al. 2010). A narrow scope can neglect important details, as even the stellar mass function can vary with environment (e.g. Yang, Mo & van den Bosch 2009; Wetzel et al. 2013; Montero-Dorta et al. 2021), for example.

Dwarf galaxies can provide a significant additional calibration for simulations. They have, by definition, low masses, and therefore shallow potential wells, which makes their star formation histories particularly sensitive to key processes like feedback (e.g. Lacey & Silk 1991; Read & Gilmore 2005; Hopkins et al. 2012; Oñorbe et al. 2015; Davis et al. 2022). Additionally, gas loss via ram pressure stripping (RPS) is very efficient in dwarfs (Boselli et al. 2008; Toloba et al. 2015; Venhola et al. 2019; Boselli, Fossati & Sun 2022), and tidal interactions tend to be more effective at disrupting them or rearranging mass within them than in higher mass galaxies (Moore et al. 1998; Mastropietro et al. 2005; Koch et al. 2012; Jackson et al. 2021a; Montes et al. 2021; Jang et al. 2024). Dwarf galaxies are also the most common kind of galaxy by number in all environments (Driver et al. 1994; Blanton et al. 2005; McNaught-Roberts et al. 2014; Kaviraj et al. 2017), meaning that they can provide a large, robust sample from which to draw conclusions about the physics driving galaxy evolution.

A comparison between real and simulated dwarfs is thus an effective means of calibrating a simulation at a granular level. Beyond the stellar mass function, galaxies follow scaling relations between stellar mass, size, surface brightness, light concentration, and other structural properties (e.g. Okamura, Kodaira & Watanabe 1984; Bershady, Jangren & Conselice 2000; Conselice 2003; Shen et al. 2003; Saintonge et al. 2008; Holwerda et al. 2014; van der Wel et al. 2014; Paulino-Afonso et al. 2019; Trujillo, Chamba & Knapen 2020). Following the evolution of these relations through cosmic time and across environments probes how they must arise from the same self-regulated evolution of baryonic mass that drives the stellar mass function (e.g. Trujillo et al. 2006; Szomoru, Franx & van Dokkum 2012; Huertas-Company et al. 2013; Taylor & Kobayashi 2016; Hamadouche et al. 2022). The 2D distribution of baryons is thus a more stringent test of a simulation's efficacy. Reproducing outliers from these relations (e.g. dwarfs with large size and low surface brightness; Sandage & Binggeli 1984; Impey, Bothun & Malin 1988) may be even more critical, as such galaxies could be the most sensitive probes of feedback and gravitational physics available (e.g. Di Cintio et al. 2017; Jackson et al. 2021b).

Ideally, an investigation into dwarf galaxies would use samples spanning many environments, from voids to massive clusters. However, obtaining accurate distances to dwarfs is a time-intensive process (e.g. Zaritsky et al. 2022), and so surveys targeting dwarf galaxies are often centred around massive systems with which the dwarfs can be associated spatially (e.g. Geha et al. 2017; Venhola et al. 2018; Trujillo et al. 2021). In such cases, the impacts of baryonic feedback on dwarf galaxy structure cannot be easily isolated from those of environment (e.g. Watkins et al. 2023; Kaviraj et al. 2025). That said, clusters and massive groups – representing the most extreme density environments – tend to produce extreme impacts on their dwarf populations (Sandage & Binggeli 1984; Ferguson & Sandage 1990; Lisker et al. 2006; Janz et al. 2021; Romero-Gómez et al. 2024), and of course contain large numbers of galaxies of all stellar mass, including dwarfs. Thus, for a comparison between simulations and observations, clusters and massive groups do offer the following: abundant populations of heavily processed dwarfs, complete down to low stellar mass.

We thus compare the structural scaling relations of dwarf galaxies found in the two most massive haloes in the NEWHORIZON simulation (Dubois et al. 2021) with the dwarf sample unveiled in the Fornax Cluster by Venhola et al. (2018), the Fornax Deep Survey (FDS; Peletier et al. 2020) Dwarf Galaxy Catalog (FDSDC). Comparisons with the FDSDC benefit from its abundant supply of dwarfs in a dense environment nearby enough that detailed structural decompositions are possible (e.g. Su et al. 2021). We begin, in Section 2, with a brief overview of both the NEWHORIZON simulation and the FDS. We then describe the methods by which we construct and analyse synthetic observations from NEWHORIZON in Section 3. We compare the simulated dwarf and FDS dwarf scaling relations in Section 4. We explore potential reasons for the differences we uncover between FDS and NEWHORIZON dwarfs in Section 5. Finally, we summarize the paper in Section 6.

2 SIMULATED DATA AND OBSERVATIONS

2.1 NEWHORIZON simulation

NEWHORIZON is a zoom-in simulation of a spherical region with a diameter of 20 Mpc within its parent, HORIZON-AGN (Dubois et al. 2014; Kaviraj et al. 2017), large enough for a 4096^3 resolution (cells; in terms of dark matter mass, $M_{\rm DM} = 1.2 \times 10^6\,{\rm M}_\odot$). NEWHORIZON thus uses the same cosmological model as HORIZON-AGN, with parameters compatible with the 7-year *Wilkinson Microwave Anisotropy Probe* (*WMAP*-7; Komatsu et al. 2011): matter density $\Omega_{\rm m} = 0.272$, dark energy density $\Omega_\Lambda = 0.728$, amplitude of the matter power spectrum $\sigma_8 = 0.81$, baryonic density $\Omega_{\rm b} = 0.045$, Hubble constant $H_0 = 0.74\,{\rm km\,s^{-1}\,Mpc^{-1}}$, and scalar spectral index $n_{\rm s} = 0.967$.

NEWHORIZON is run with the adaptive mesh refinement RAMSES code (Teyssier 2002), resulting in a maximum spatial resolution of 34 pc within a contiguous $(16\ {\rm Mpc})^3$ volume. Combined with the very high stellar mass resolution ($1.3 \times 10^4\,{\rm M}_\odot$), this makes the simulation very useful for the study of dwarf galaxies. One limitation of our study, however, is that of environment, as the volume sampled is not large enough to include any clusters with Fornax-like halo masses. Instead, we draw our dwarf population from NEWHORIZON's two largest groups, with halo masses of $6 \times 10^{12}\,{\rm M}_\odot$ and $7 \times 10^{12}\,{\rm M}_\odot$. These are approaching the mass of Fornax ($7 \pm 2 \times 10^{13}\,{\rm M}_\odot$; Drinkwater, Gregg & Colless 2001), but are about an order of magnitude smaller. We consider the implications of this difference throughout our study.

Star formation in NEWHORIZON occurs above a gas density threshold of $n_0 = 10$ cm^{-3}, following a Schmidt relation (Schmidt 1959) wherein the star formation rate (SFR) is proportional to the gas density and inversely proportional to the local free-fall time, with a variable efficiency (Padoan & Nordlund 2011; Federrath & Klessen 2012; Kimm et al. 2017). Likewise, the turbulent Mach number is determined by the local 3D instantaneous velocity dispersion. SFRs (and, consequently, feedback) can occur at higher gas densities and thus achieve higher values than in its parent simulation, depending on local conditions.

Feedback itself is limited to Type II supernovae (SNe) and active galactic nuclei (AGNs). The latter is unimportant in the simulated dwarf regime (the requisite black holes tend not to grow in NEWHORIZON dwarf galaxies; Jackson et al. 2021b), and hence will not be considered here. The former releases 10^{51} erg of kinetic energy per explosion, assuming a lower limit of $6\,M_\odot$ for stars that can explode. The frequency of such stars assumes each star particle ($10^4\,M_\odot$) is composed of a simple stellar population (SSP) following a Chabrier initial mass function (IMF) with a mass range of $0.1 < M/M_\odot \leq 150$ (Chabrier 2005). Momentum is transferred via the mechanical SN feedback scheme of Kimm & Cen (2014) and Kimm et al. (2015).

NEWHORIZON reproduces many observed galaxy scaling relations to good accuracy, particularly at the high-mass scale. This includes, for example, the galaxy mass function, the cosmic SFR and stellar density, the Kennicutt–Schmidt relation (Schmidt 1959; Kennicutt 1998), the Tully–Fisher relation (Tully & Fisher 1977), the massive black hole–galaxy mass relation (Dubois et al. 2021), and many others using integrated quantities.

2.2 Fornax Deep Survey

We compare the simulated dwarfs from NEWHORIZON with observed dwarfs found in the Fornax Cluster via the FDS, which combines data from the VLT (Very Large Telescope) Survey Telescope (VST) Early-Type GAlaxy Survey (VEGAS, PIs: M. Capaccioli and E. Iodice), and the FOrnax Cluster Ultra-deep Survey (FOCUS, PI: R. F. Peletier; Capaccioli et al. 2015). Both of these were conducted with the VST's square-degree OmegaCAM (Kuijken et al. 2002) camera at the European Southern Observatory, targeting both the Fornax Cluster itself (26 deg^2 centred on the brightest cluster galaxy NGC 1399 in g', r', and i', and 21 deg^2 in u') and its associated subgroup Fornax A. In the three deepest photometric bands (g', r', and i'), the FDS reaches limiting surface brightnesses >30 mag arcsec^{-2} (3σ, 10×10 arcsec^2; Venhola et al. 2018). Iodice et al. (2016) and Venhola et al. (2018) provide a detailed account of the survey's observation strategy and data reduction procedure. For all of our derived quantities, we assume a distance to the Fornax Cluster of 20 Mpc (Blakeslee et al. 2009).

For our study, we used the photometric parameters derived for the FDSDC (Venhola et al. 2018) by Su et al. (2021) and later Watkins et al. (2023) using a combination of radial profiles and Sérsic and point spread function (PSF) decompositions. The catalogue contains such parameters for 564 dwarf galaxies in Fornax with stellar masses as low as $10^5\,M_\odot$ (with said stellar masses estimated from $g' - i'$ and $r' - i'$ colours using the calibrations from Taylor et al. 2011).

For our comparison with NEWHORIZON, we limit the sample to galaxies with stellar masses $>10^7\,M_\odot$ (corresponding to $\sim$1000NEWHORIZON star particles), as any simulated dwarfs with masses lower than this will not be very well resolved. While the Su et al. (2021) catalogue does not include the 265 additional dwarfs identified later by Venhola et al. (2022), only seven additional galaxies with $\log(M_\star/M_\odot) > 7$ were found among the latter, meaning the resolution limits of NEWHORIZON preclude a realistic comparison with most of these newly uncovered dwarfs. The Su et al. (2021) catalogue still contains 250 galaxies with masses in the range $7 < \log(M_\star/M_\odot) < 9.5$, significantly more than either NEWHORIZON group (likely due to Fornax's larger halo mass), hence our study is limited (in terms of number statistics) mostly by the simulated catalogue.

3 METHODS

Here, we briefly summarize the methods we employed to create synthetic observations from the NEWHORIZON simulation and to derive structural parameters from those synthetic observations. We note that we include all of the massive ($\log(M_\star/M_\odot) > 9.5$) FDS and NEWHORIZON group galaxies alongside our analysis of dwarfs, as NEWHORIZON uses the massive galaxy population as their typical benchmark for observational comparisons.

3.1 Synthetic image generation

To compare the photometric properties of simulated dwarfs with those of real dwarfs, we constructed synthetic observations of all dwarf (and massive) galaxies found within the two largest haloes in the NEWHORIZON simulation. We did this following the process outlined by Martin et al. (2022), with parameters meant to replicate the observations made for the FDS. While we provide a brief summary here, for a full description of the image-generation process, we refer the reader to that paper. Additional details will be elaborated on by Martin et al. (in preparation).

We first extracted all star particles within a 20 kpc radius centred on each galaxy with stellar mass above $M_* = 10^{10}\,M_\odot$, or a 10 kpc radius otherwise. As this does not exclude any particles within that volume, we are not reliant on any specific galaxy identification methodology, other than the values of stellar mass and centroid; we discuss one consequence of this in Section 3.2. As each particle is described by an age and a metallicity, we derived particle-by-particle spectral energy distributions (SEDs) via interpolation of a grid of SSP models from Bruzual & Charlot (2003), assuming a Chabrier (2003) IMF, which is also what was used to calculate the integrated stellar masses we compare against. We used a screen dust model along the line of sight to each particle to simulate the attenuation of these SEDs, where the dust column density is given by

$$N_{\rm cell} = \rho Z \Delta r \times {\rm DTM}. \quad (1)$$

Here, ρ is the gas density in the adaptive mesh refinement cell, Z is the gas-phase metallicity, Δr is the line-of-sight cell length, and DTM is the dust-to-metal ratio. For the latter, we used two values: above $\log(M_*/M_\odot) \geq 10$, we adopted the value from Martin et al. (2022) of DTM = 0.4 (Draine et al. 2007); below this, we used DTM = 0.1. The latter we chose based on the relation between DTM and metallicity shown in fig. 4 of Li, Narayanan & Davé (2019), using the median galaxy mass in our simulated sample of $\log(M_*/M_\odot) = 8$, and the mass–metallicity relation for dwarfs shown in fig. 6 of Buzzo et al. (2024).

We then produced dust-attenuated SEDs as

$$I(\lambda)_{\rm attenuated} = I(\lambda)\,{\rm e}^{-\kappa(\lambda)N}, \quad (2)$$

where $\kappa(\lambda)$ is the dust opacity, and N is the total column density in front of each star particle, summed along the line of sight. We derived dust opacities from the Weingartner & Draine (2001) extinction curves, using the Milky Way (MW) $R_V = 3.1$ curve for galaxy

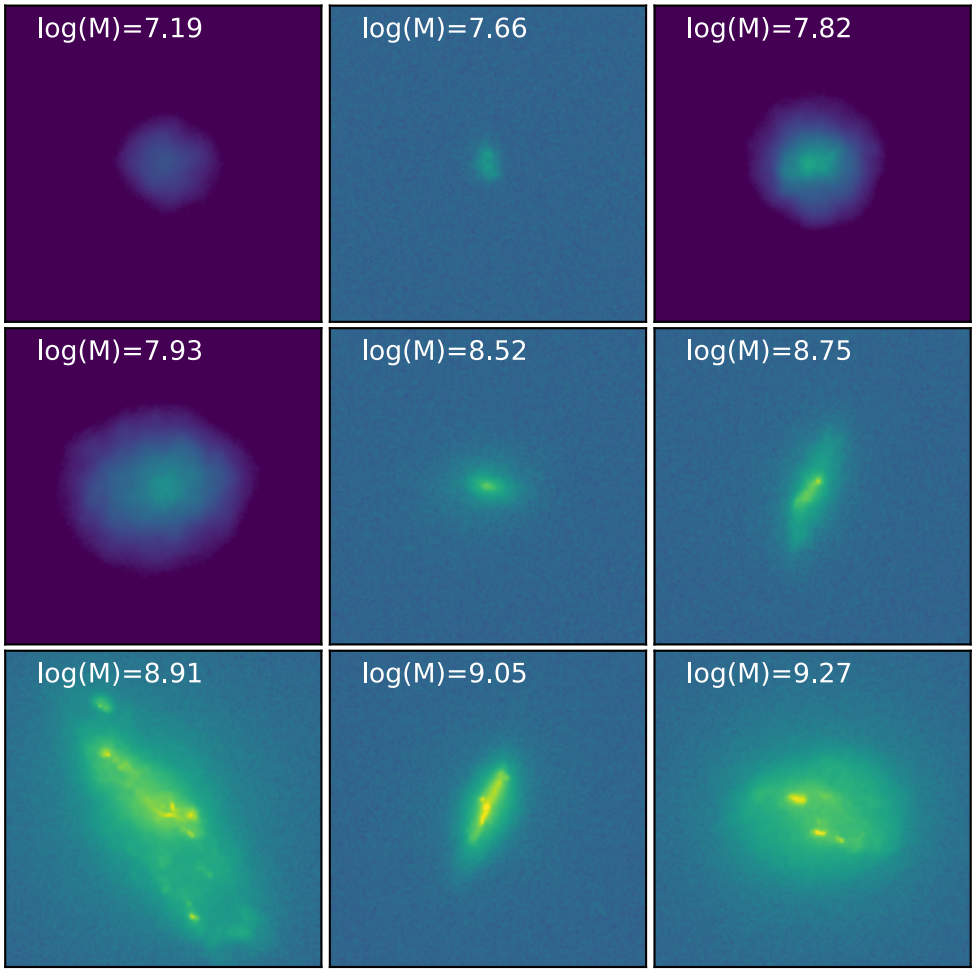

Figure 1. Nine example stamps made of synthetic NEWHORIZON dwarfs, at the final NEWHORIZON time-step ($z = 0.17$). All images are scaled such that the width is 10 kpc, and the surface brightness spans $\mu_{r'} = 29.5$–21 mag arcsec^{-2}. We mark the galaxy stellar masses in the upper left of each panel, in units of log($M_\odot$). Panels with dark backgrounds (top and middle left, top right) show examples of galaxies too faint to be detected using the FDS sky background (around half the sample; see text), whose background we adjusted to be arbitrarily low noise.

masses above $\log(M_*/M_\odot) \geq 10$, and the Small Magellanic Cloud (SMC) bar extinction curve below this. Magnitudes and luminosities were derived by convolving these attenuated SEDs (corrected for redshift) with the g' and r' filter transmission curves. We show examples of nine NEWHORIZON galaxy stamps created through this process in Fig. 1.

We note that the choice of DTM and extinction curve has little impact on the magnitudes and surface brightnesses we derived. Varying the DTM from 0.01 to 1.0, and using either MW or SMC extinction curves results in variation in total magnitudes of order 0.005 mag and in central surface brightnesses of order 0.01 mag arcsec^{-2} in both g' and r'. This is likely because these galaxies are located in massive groups and so are relatively gas-poor compared to the field population. Likewise, we expect using full radiative transfer rather than a screen dust model would not impact our conclusions (see e.g. fig. 5 of Kaviraj et al. 2017). We find that the use of a Salpeter (1955) IMF primarily affects the bluest galaxies, decreasing their magnitudes by $\sim$1 in either band and their surface brightnesses by $\sim$0.6 mag arcsec^{-2} (echoing Martin et al. 2022). Red galaxies are mostly unaltered.

For low-density regions within the galaxies, we applied the same adaptive smoothing algorithm used by Martin et al. (2022),[1] which follows a method similar to that of ADAPTIVEBOX, employed by Merritt et al. (2020). In summary, we split each star particle in these low-density regions into 500 equal flux particles with normally distributed positions, centred at the original particle position with a standard deviation equal to the particle's fifth nearest neighbour distance, then generated the image by summing the subparticle fluxes along a chosen axis. The latter step employs a 2D grid with elements 0.2×0.2 arcsec^2, following the FDS pixel scale. We then created image stamps of these flux-scaled, smoothed particle distributions, along the simulation's x–y axis (an arbitrary choice, meaning the galaxy orientations are random). While the particle data are drawn from the simulation's final time-step of $z = 0.17$, we scale the size and flux of each galaxy to $z = 0.0047$, which yields a distance modulus of 31.51 (echoing Blakeslee et al. 2009) using the *WMAP*-7 (Komatsu et al. 2011) cosmological parameters. At this scale, one pixel is $\sim$20 pc, which is smaller than the highest resolution cells in the NEWHORIZON simulation; however, we found by creating a

[1] https://github.com/garrethmartin/smooth3d

subset of more distant stamps that this has little impact on our derived photometric quantities.

Once stamps of the simulated galaxies are created in this way, we apply image characteristics to them similar to the FDS coadds used by Venhola et al. (2018) to construct the FDSDC. These coadded images have a pixel scale of 0.2 arcsec pixel^{-1}, with all flux scaled such that the AB magnitude zero-points are 0.0 in all photometric bands. To mimic the survey resolution, we convolved the simulated galaxies in our images with the analytic PSF models published by Venhola et al. (2018). These models are composed of Gaussian and Moffat profile cores (their equation 5), with wings modelled as declining exponential functions (their equation 6, extending to 160 arcsec radius). Given that the PSF is variable from field to field, we used the PSF parameters for Field 11 (table A2 of Venhola et al. 2018), in the centre of Fornax, to construct our model FDS PSFs for each photometric band. As both Venhola et al. (2018) and Su et al. (2021) used only the g' and r' bands for their photometric analysis, we constructed only these images for the NEWHORIZON sample.

Also following Martin et al. (2022), we added synthetic sky-subtracted backgrounds to all mock exposures using the coadded images' limiting surface brightnesses converted to a per pixel 1σ variance (their equation 3, derived from appendix A of Román, Trujillo & Montes 2020). These are $\mu_{\mathrm{lim},\,g'} = 28.4$ mag arcsec^{-2} and $\mu_{\mathrm{lim},\,r'} = 27.8$ mag arcsec^{-2} (1σ, 1×1 arcsec^2; Venhola et al. 2018). However, 43 of the NEWHORIZON galaxies were too faint to be detectable at this surface brightness, so for these we used an arbitrary background of $\mu_{\mathrm{lim},\lambda} = 32$ mag arcsec^{-2} to avoid throwing out nearly half the sample.

3.2 Photometry and decompositions

Having produced mock FDS observations of the NEWHORIZON galaxies, for a fair comparison, we needed to derive their photometric properties in the same ways in which they were derived for the real FDS dwarfs. The photometric techniques employed by Su et al. (2021) for the FDS galaxies follow those developed for the *Spitzer* Survey of Stellar Structure in Galaxies (Sheth et al. 2010) by Muñoz-Mateos et al. (2015) and Salo et al. (2015). Again, we provide only a brief summary of these methods here, pointing out any differences in technique we employ for this work; a full description can be found in the papers cited above.

From every synthetic NEWHORIZON exposure, we derived radial surface brightness profiles and curves of growth, from which we derived integrated properties such as the effective radius. We measured these profiles using the ASTROPY-affiliated package PHOTUTILS's (v.1.11.0; Bradley et al. 2024) isophote-fitting algorithm ELLIPSE, itself based on the IRAF routine of the same name (Jedrzejewski 1987; Busko 1996).

We first fit the galaxies using free parameters to establish their characteristic isophotal shapes. For each galaxy, we estimated the galaxy centres initially using the PHOTUTILS centre-of-mass centroiding algorithm within a 20×20 pixel box at the image centre. We then ran ELLIPSE multiple times per galaxy, cycling through a handful of starting isophotal parameter [semimajor axis length, position angle (PA), and ellipticity] combinations until each fit proceeded successfully. Unlike in real images, which contain masked interloping sources, correlated noise, and other similar features, we found that successful fits were robust to these starting parameters, so no fine-tuning was necessary. If a fit proceeded with a set of starting parameters, it would proceed identically on a successful fit using a different set of starting parameters.

With free-parameter fits made, we again measured the radial profiles using fixed isophote shapes derived from the outer regions of each galaxy (see Muñoz-Mateos et al. 2015). We chose these by examining each galaxy's free-parameter radial PA and ellipticity (ϵ) profiles, hand-selecting radius ranges where these parameters were roughly constant, and taking the median PA, ϵ, and centre coordinates measured within those limits as the characteristic isophotal parameters for the galaxy. This was often difficult, as unlike the Fornax galaxies, almost all of these synthetic galaxies showed highly variable isophote shapes with radius. To assist with this, we also created deprojected images of each galaxy using these parameters by transforming each image's Cartesian coordinates into elliptical coordinates, accepting the parameters as valid only if these deprojected galaxy images appeared roughly circular. We derived all photometric quantities (such as R_{eff}) from either the surface brightness profiles or curves of growth measured from the standard projection images using the fixed isophotal parameters derived in this way.

Normally, prior to measuring magnitudes, sizes, and so on via the resulting curves of growth, a local background estimate is made and subtracted by measuring flux in apertures near the galaxies but visibly dominated by background noise. As we injected backgrounds with zero mean flux into our synthetic images, initially we deemed such a correction unnecessary. However, we found through examination of skyless stamps that many dwarfs are embedded in a near-uniform, diffuse medium at very low surface brightness ($\mu_r > 32$ mag arcsec^{-2}), which contributes non-negligible flux to the lowest mass dwarfs when its contribution is summed over large concentric annuli. This originated from how we built our stamps; as stated in Section 3.1, we did not exclude any particles within a 10 kpc (20 kpc for massive galaxies) radius volume around each galaxy. We therefore apply background corrections to our photometry, measured in boxes placed at the stamp edges, to correct for this. The necessity of such corrections implies a systematic uncertainty on our measurements which is not present when estimating simulated galaxy sizes via the particle distributions or structure finder directly, but which is always present when using similar techniques on images of real galaxies.

Su et al. (2021) also performed Sérsic profile decompositions using the two-dimensional fitting algorithm GALFIT (Peng et al. 2002, 2010). We did this as well, first deriving single-component decompositions for all galaxies, then multicomponent decompositions for each galaxy which seemed to merit additional components based on the appearance (from visual inspection) of the residuals from the best-fitting single-component models. If the stamp contained an obvious companion galaxy, we fit both simultaneously. We used these to estimate Sérsic indices and central surface brightnesses of the galaxies and to compare the frequency with which multicomponent fits are required for NEWHORIZON dwarfs compared to Fornax dwarfs.

GALFIT requires two templates for optimal fitting results: a normalized PSF model and a sigma image (used to weight each pixel in the fit; see Peng et al. 2002). For the former, we used the models with which we convolved the simulated galaxies described in the previous section. For the latter, we derived weights for each pixel using the following equation:

$$\sigma(x, y) = [(\mathrm{gain} \times (I(x, y) + S))^2 + \mathrm{RON}^2]^{1/2}, \quad (3)$$

where the gain is the camera gain in electrons per analogue-to-digital unit (e$^-$ ADU^{-1}), $I(x, y)$ is the synthetic galaxy's intensity at pixel (x, y) in ADU, S is a constant sky brightness in ADU, and RON is the readout noise in e$^-$. We used the mean of the gains found in the headers of the FDSDC stamps we had available as the gains per

band, and we set the RON to 4.4 e^-, the mean of 19 CCDs in VST's OmegaCam.[2] For S, we used the mean sky brightnesses for g' and r' published in table 2 of Yoachim et al. (2016), converted to ADU.

We found using a handful of stamps that GALFIT produces very similar fits when using its own auto-generated sigma images compared to those we supply, assuming the proper information is present in the stamp headers. Supplying our own sigma images, therefore, serves mostly to speed up the fitting procedure. Likely this is due to the idealized nature of the synthetic exposures, which lack artefacts, masked pixels, and have perfectly Gaussian noise backgrounds by construction. We also found that the GALFIT results, if the fits succeeded, were insensitive to the initial parameters supplied, other than the number of iterations required to reach a minimum in the χ^2 between the model and the image.

Five of the NEWHORIZON galaxies appeared to be extremely diffuse and without any discernible structure. These have anomalously faint magnitudes for their stellar masses and are not well characterized by Sérsic profiles. Indeed, their light profiles are not monotonically declining, meaning derived parameters, such as total magnitude (and thus, half-light radius), are ambiguous at best. We have verified that the fraction of low-resolution dark matter particles is zero among all group galaxies we study, including these (see also Jang et al. 2024), thus they do not appear to be dwarf galaxies altered by resolution effects. Likely these were simply identified as local peaks within extremely underdense regions of the galaxy groups by the structure finder (possibly tidal features or intragroup light); hence, we remove these from our sample. Likewise, some dwarfs were embedded within the isophotes of companion galaxies; for these, we use the GALFIT magnitudes and sizes, rather than the curve of growth measures, as the latter is contaminated by the companion's light. Finally, the NEWHORIZON sample contains 10 extremely compact objects reminiscent of ultracompact dwarfs (UCDs; Drinkwater et al. 2000), which are not present in the FDSDC (although they are present in the Fornax Cluster itself). As our interest here is normal dwarf galaxies, we identify these as $>5\sigma$ outliers from the half-light radius–stellar mass relation and remove them from the sample as well. NEWHORIZON UCDs are discussed in detail by Jang et al. (2024).

4 RESULTS

Fig. 2 shows a variety of correlations between derived galaxy properties in the form of a corner plot. In each panel, black dots denote NEWHORIZON galaxies, while red triangles denote Fornax Cluster galaxies. Histograms of each distribution along the diagonal are similarly colour coded. Descriptions of the parameters plotted are provided in the figure caption. Here we relate the most significant similarities and differences between the simulated and observed cluster galaxies.

At stellar masses below $\log(M_\star/\mathrm{M}_\odot) \lesssim 9$, we find a slight ($\sim$1 mag) offset in the mass–magnitude relation, where agreement is much better above this threshold. Use of a Salpeter IMF does not affect this offset at the low-mass end, but does create a similar offset at higher stellar masses. This implies that NEWHORIZON dwarfs are underluminous compared to their Fornax counterparts. Partly this may be an artefact of our derivation of SEDs using the Bruzual & Charlot (2003) SSP models, which span a limited number of metallicities.

[2]https://www.eso.org/sci/facilities/develop/detectors/optdet/docs/papers/omegacam_poster.pdf

Dwarfs show an offset in the mass–size relation between NEWHORIZON and FDS. For galaxies below $\log(M_\star/\mathrm{M}_\odot) \lesssim 9.5$, $R_{\rm eff}$ is systematically too high among NEWHORIZON galaxies. Here, the mass–size relation is roughly horizontal at $R_{\rm eff} \sim 3$ kpc, while the FDS dwarfs show a distinct positive correlation between $R_{\rm eff}$ and stellar mass despite the somewhat large scatter. We note this size offset can also be seen in fig. 4 of Jang et al. (2024).

NEWHORIZON dwarfs also have much smaller 25 mag arcsec^{-2} isophotal radii ($R_{25,\,r'}$) than the FDS dwarfs. This is due to their lower surface brightnesses: NEWHORIZON shows mostly parallel μ–$\log(M_\star)$ relations to FDS, offset to fainter values (although the matches appear better at higher stellar mass). Here, the offset is much larger than that with magnitude, at 3–4 mag arcsec^{-2}. This is larger for central surface brightness μ_0, which can be seen as a slight offset between FDS and NEWHORIZON in the $\mu_{0,\,r'}$–$\mu_{\rm eff,\,r'}$ relation, suggesting that the offset is not uniform with radius. Correcting dwarf surface brightness by increasing $m_{r'}$ to match the FDS $m_{r'}$–$\log(M_\star)$ relation only improves the match slightly, implying that it is the larger values of $R_{\rm eff}$ causing this difference.

The distribution of Sérsic indices (n) among NEWHORIZON and FDS dwarfs is fairly similar, scattering mostly around $n = 1$, though NEWHORIZON dwarfs appear to trend slightly below their FDS counterparts. FDS dwarfs show a slightly positive trend in n with stellar mass (for a discussion of this, see Watkins et al. 2023), which is absent among the NEWHORIZON dwarfs. In general, however, NEWHORIZON and FDS show a fairly good match in terms of dwarf light profile shapes (despite, as stated above, the normalizations of those profiles being different).

NEWHORIZON dwarfs show a wider range of integrated colour ($g' - r'$) than their FDS counterparts. Most of the NEWHORIZON dwarfs in these groups appear quenched below $\log(M_\star/\mathrm{M}_\odot) \lesssim 8.5$, with uniformly red colours. These still lie at the blue end of the FDS colour distribution. While this may imply that NEWHORIZON dwarfs are lower in metallicity, it may be another artefact of our use of the Bruzual & Charlot (2003) models to generate the mock SEDs. Above this mass threshold, most NEWHORIZON galaxies are significantly bluer than those in Fornax, implying higher SFRs. This may be a result of the differences in halo mass: these groups are both a factor of $\sim$10 lower in virial mass than the Fornax Cluster, implying that RPS is not as efficient here.

Finally, we find that 20 per cent of the NEWHORIZON dwarf galaxies require multiple components when fitting GALFIT models, always in the form of central light concentrations. From Su et al. (2021), 25 per cent of the Fornax dwarfs have bright, compact nuclei, a comparable fraction.

In summary, NEWHORIZON dwarfs are fainter, more radially extended, lower in surface brightness, and bluer in colour than FDS dwarfs at the same stellar mass, despite having similar roughly exponential light profile shapes. We explore possible reasons for these differences in the next section.

5 DISCUSSION

NEWHORIZON dwarfs in the two largest groups found in the simulation are larger and more diffuse than Fornax Cluster dwarfs of the same stellar mass. Here, we explore the most likely reasons for these differences. We split these into two broad categories: environment (including RPS and tidal interactions) and internal processes (feedback). Throughout, we also consider the joint impact of these two factors, as well as the issue of the simulation's resolution.

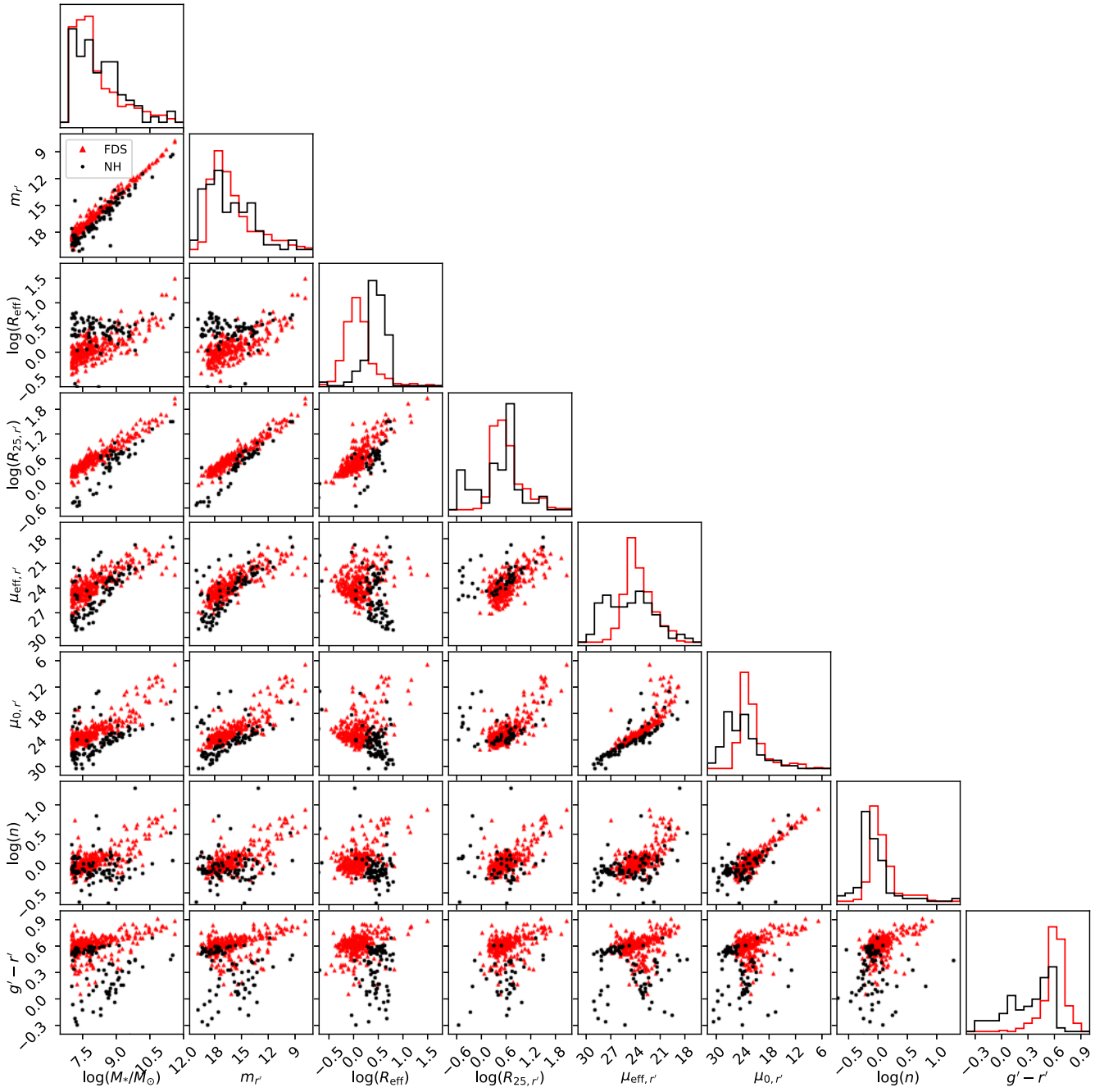

Figure 2. A corner plot, showing the correlations between eight different variables. From the left to right along the bottom axis, these are: stellar mass (in $M_\odot$), integrated r'-band magnitude, effective radius (kpc, estimated along the major axis), the $\mu_{r'} = 25$ mag arcsec^{-2} isophotal radius (kpc, with surface brightness corrected for inclination using the axial ratio), mean surface brightness within the effective radius, central surface brightness, Sérsic index, and integrated $g' - r'$ colour. In all panels, black dots or histograms indicate NEWHORIZON synthetic galaxies, while red triangles or histograms indicate FDS galaxies. All sizes and other photometric quantities here were derived in the r' photometric band.

5.1 Environmental influence

Perturbations from neighbouring galaxies, including fly-by interactions and merger events (in which two or more galaxies coalesce), can provide kinematic kicks to their existing gaseous, stellar, and dark matter components. The impact on gas is different than on the collisionless stellar and dark matter components, as gas is able to radiatively cool and condense at high enough densities (e.g. Lucy 1977; Hernquist & Katz 1989). The impact of tidal perturbations on gas thus, broadly, leans towards compression and cooling, leading to temporary enhancements in star formation. Most often this enhancement occurs in the galaxy core in conjunction with SFR suppression in the outskirts, as gas loses angular momentum in response to torques (e.g. Keel et al. 1985; Mihos & Hernquist 1994; Ellison et al. 2008; Moreno et al. 2015; Williamson et al. 2016; Daikuhara et al. 2024). One might naively expect that interaction-induced star formation should ultimately serve to enhance the central densities of galaxies, decreasing their $R_{\rm eff}$ and increasing $\mu_{\rm eff}$ or

μ_0. However, this study demonstrates that the NEWHORIZON dwarfs show the opposite trend compared to the observed dwarfs.

The impact of tides on collisionless particles (stars and dark matter) depends on the parameters of the interaction. For a given two-body system, the duration over which the tidal force is present determines the extent to which stellar orbits alter in response. For example, whether an encounter is prograde or retrograde affects the length and thickness of any resulting tidal arms (Toomre & Toomre 1972). Stars in a dwarf or globular cluster plunging through a more massive galaxy can also increase their velocity dispersion if they do not have enough time to adapt to the rapidly changing gravitational potential (i.e. their dynamical times are long compared to the gravitational impulse, a process known as tidal shocking; Ostriker, Spitzer & Chevalier 1972). Stars within $1R_{\rm eff}$, with short dynamical times, are less impacted by tides. In the most extreme such cases, the most loosely bound stars will become unbound (e.g. Peñarrubia, Navarro & McConnachie 2008), although on non-radial orbits this may require several pericentric passages given the stability provided by their dark matter halo. Broadly, such interactions tend to result in a <1 per cent loss in stellar luminosity even in the dwarf regime (e.g. Mihos 2004; Martin et al. 2022).

Stellar velocity dispersion can also increase in response to a sudden dramatic mass loss, such as the loss of gas during RPS (e.g. Hammer et al. 2024). This is simply a gravitational response to the decreased potential well depth, as, assuming no external tidal perturbation, the stars in systems undergoing RPS retain their original orbital velocities. However, in a simulation by Boselli et al. (2008), it was found that the impact of RPS on cluster dwarf structures at long wavelengths (H band) was negligible, while at shorter wavelengths, RPS ultimately resulted in decreased surface brightness (due to truncated star formation) and effective radius (due to an enhanced SFR ratio between the core and the disc). The ultimate impact of RPS on the dwarf structure thus depends on whether or not the gas is removed predominantly via the stripping itself (thereby altering the dwarf's gravitational potential), or via enhanced star formation induced by the ram pressure (thereby merely rearranging the existing mass within said potential).

Additionally, the environment impacts the amount of fuel available for star formation, especially at high redshift. Denser regions promote initially faster gas infall, resulting in higher initial SFRs. If this star formation is then later truncated by interactions or RPS within said dense environment, these initial conditions can impact the evolutionary end state of the galaxies (e.g. Martin et al. 2019; Jackson et al. 2021b). In this way, environment and baryonic feedback can end up coupled.

That said, observations indicate that the scaling relations we investigate here may not be strongly correlated with the environment. Habas et al. (2020) and Poulain et al. (2021) showed that their sample of dwarfs from the MATLAS (Mass Assembly of early-Type GaLAxies with their fine Structures) survey (Duc et al. 2015), preferentially surrounding massive early-type galaxies, falls along the same magnitude–$R_{\rm eff}$ and magnitude–surface brightness relations as cluster, Local Volume, and Local Group dwarfs. We show similar results in Fig. 3, which compares the correlations between $\mu_{\rm eff}$ and $R_{\rm eff}$ with stellar mass across four different studies. As in Fig. 2, we show the FDS relation as red triangles and our NEWHORIZON group dwarf relation as black points. Purple crosses denote measurements from Carlsten et al. (2021), for a sample of Local Volume satellite dwarfs. Orange squares denote measurements for NEWHORIZON galaxies in the two most massive groups by Jackson et al. (2021b), who estimated surface brightnesses using the unattenuated intensity-weighted second moments of the particle distribution rather than via 2D analysis of mock images (as we did). Orange contours underlying these points showcase the entire NEWHORIZON galaxy population from Jackson et al. (2021b). Blue squares are values from the $z < 0.08$ field dwarf galaxy sample from Lazar et al. (2024a, b) derived from the COSMOS2020 catalogue (Weaver et al. 2022). The coloured dashed lines represent the running medians of the corresponding data sets. For better comparison, we include the full range of stellar masses from Venhola et al. (2018) for the FDS sample in this figure.

Despite the different techniques used for estimating $\mu_{{\rm eff},\,r'}$, our NEWHORIZON$\mu_{{\rm eff},\,r'}$–log($M_\star$/M$_\odot$) relation aligns well with that from Jackson et al. (2021b). Both of these lie systematically below the relations derived from observations at low stellar mass, all of which agree well between studies despite the differences in sampled populations. This implies that the structural differences we find between NEWHORIZON and observed dwarfs are not limited to those found in the massive haloes. While tidal interactions and RPS can influence dwarf structure, it may be that the competition between the impacts of tidal disturbance or shocking (increasing stellar velocity dispersion, thus lowering surface brightness) and enhancements in SFR (increasing central stellar mass and central surface brightness) dampens the impact of these factors on the dwarf scaling relations we examine here.

We do see differences between our estimates of $R_{\rm eff}$ and those of Jackson et al. (2021b). While the two distributions match somewhat well above log($M_\star$/M$_\odot$) > 8, our size estimates consistently lie above those of Jackson et al. (2021b) for log($M_\star$/M$_\odot$) $\leq$ 8, with the disparity increasing at lower stellar mass. The 2D curve of the growth method thus appears to overestimate $R_{\rm eff}$ for low stellar mass dwarfs compared to the intensity-weighted second-moment estimates. As we mentioned in Section 3, many of our galaxy stamps show extremely faint, diffuse backgrounds extending to the edges of the stamp boundaries. While this light is extremely faint, it contributes significantly to the total fluxes of these low surface brightness dwarfs when summed up within large annulus apertures. While we attempted to subtract its influence from our curves of growth, if the regions we sampled are unrepresentative of the diffuse background cospatial with the galaxies, these corrections may not have been sufficient. Thus, this is a danger in employing standard observational photometric techniques on synthetic galaxy stamps generated in this manner. Interestingly, a recent work investigating dwarf mass–size relations using the FIREBOX simulation (Feldmann et al. 2023), which has a similar resolution to NEWHORIZON ($\sim 6 \times 10^4$ M$_\odot$ stellar mass particles), by Mercado et al. (2025) shows a distribution in $R_{\rm eff}$–log(M_*) very similar to that of Jackson et al. (2021b), implying the dwarfs are uniformly overextended in that study as well.

Detailed examination indicates that some environmental differences in these scaling relations do exist. For example, the $R_{\rm eff}$–log(M_*) relation for the field dwarf sample from Lazar et al. (2024b) is offset by $\sim$+0.5 kpc from the FDS relation (though they may simply be extending off of the known late-type galaxy relation; e.g. Muñoz-Mateos et al. 2015; Watkins et al. 2022). However, the most prominent difference is not between environments but between observed and simulated galaxy relations. Indeed, the close agreement between our $\mu_{\rm eff}$–log(M_*) relation, for NEWHORIZON dwarfs residing in the two most massive group haloes, and that of Jackson et al. (2021b), which includes all NEWHORIZON dwarfs, suggests that these simulated dwarfs are seeming as unperturbed by the environment as their observed counterparts. Also, despite the uncertainty imposed by the stamps' diffuse backgrounds, both estimates of $R_{\rm eff}$ show that NEWHORIZON dwarfs are larger everywhere.

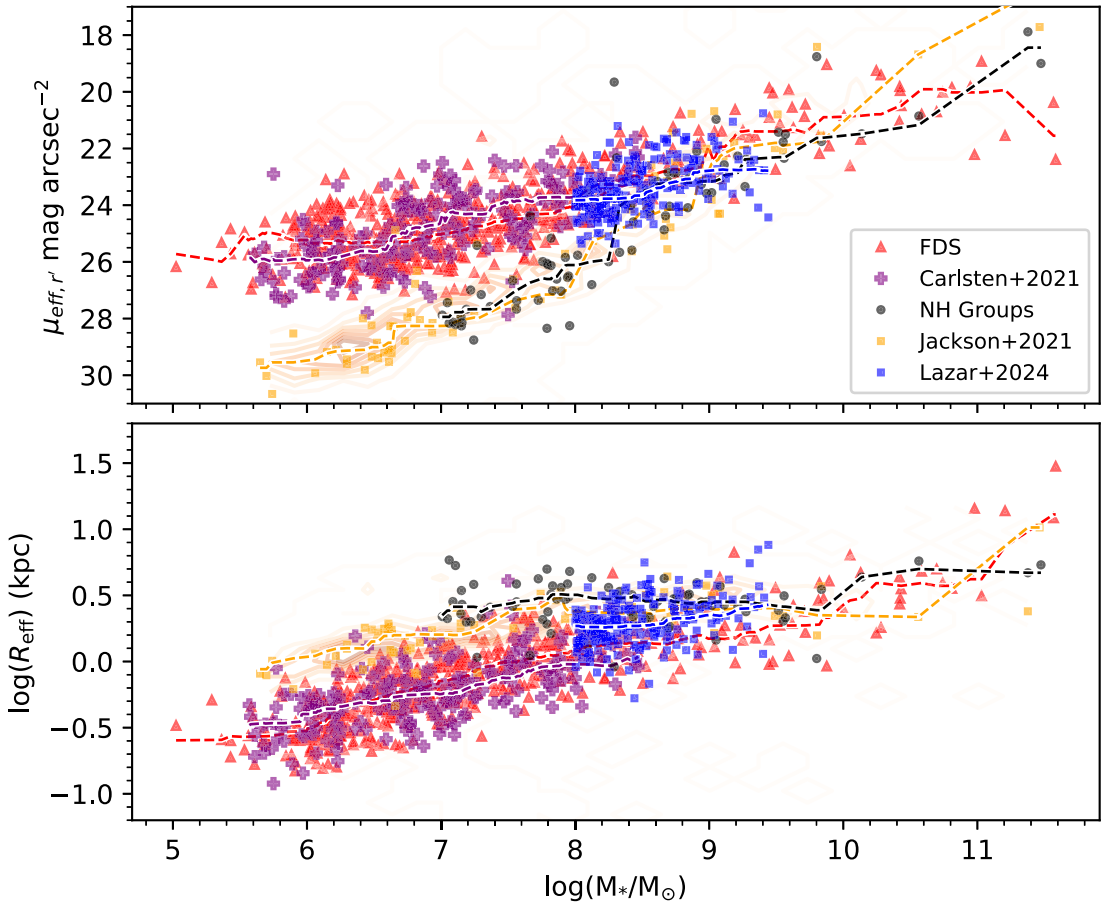

Figure 3. Comparing effective surface brightness and effective radius versus stellar mass relations from a variety of different studies. As in Fig. 2, red triangles show the FDS relation, and black points show our NH group dwarf values. Purple crosses show values for Local Volume dwarf satellites from Carlsten et al. (2021). Orange squares denote measurements by Jackson et al. (2021b) also of galaxies in the two largest NewHorizon groups, but made using the unattenuated intensity-weighted second moments of the particle distributions. Orange contours underlying these points outline the distributions for all NewHorizon galaxies from Jackson et al. (2021b). Blue squares are from Lazar et al. (2024b), for $z < 0.08$ dwarfs from the COSMOS2020 catalogue.

This is worth investigating in more detail, but for the purposes of this paper, it implies that our choice to use Fornax Cluster dwarfs does not strongly influence the comparison in this parameter space. The environmental influence appears to be subtle, with the most notable influence occurring in the faint outskirts of galaxies (e.g. Chamba, Hayes & LSST Dark Energy Science Collaboration 2024).

5.2 Baryonic feedback

If the environment has little direct impact on dwarf structure, baryonic feedback may provide most of the required energy. Feedback is necessary to counterbalance gas cooling and inflows in the early Universe (White & Rees 1978; Cole 1991), and, on more local scales, is needed to reproduce the flat, 'cored' dark matter profiles often observed through kinematics in real galaxies (e.g. Pontzen & Governato 2012; Jackson et al. 2024) and to resolve the 'missing satellite' and 'too big to fail' problems (e.g. Zolotov et al. 2012; Wetzel et al. 2016; Garrison-Kimmel et al. 2019). The broad impact of feedback is thus toward radial diffusion of stellar and dark matter profiles, leading to lower surface densities. However, precisely how this feedback impacts dwarf structure can depend on the specific subgrid physical models employed by the simulation (e.g. Crain et al. 2015; Munshi et al. 2019), including how radiative cooling and the SFR couple to the simulation's resolution (e.g. Crain et al. 2015; Benincasa et al. 2016; Ludlow et al. 2020). Isolating these effects is not a trivial task, but we can use results from previous work in the dwarf regime to aid our interpretation.

The baryonic feedback in NewHorizon is limited to two kinds: Type II SNe and AGNs (Dubois et al. 2021), both of which can transfer substantial energy and momentum into the surrounding gas (although AGN feedback in the dwarf regime here is limited due to a lack of supermassive black hole growth). The ultimate result of either mechanism is a regulation between the gas inflow rate and the SFR (e.g. Hopkins et al. 2018).

The details of this regulation matter, however. In the early stages of growth, for example, when galaxies are composed of very few particles, energy and momentum can be distributed uniformly, as smaller structures like chimneys or bubbles remain unresolved (e.g. Hopkins et al. 2018). If the gas is not replenished, the resulting galaxies will be superheated, pressure-supported systems – at later epochs, then, most of the mass build-up would be via accretion of higher angular momentum gas, resulting in more extended systems (indeed, with aggressive enough such feedback, this can even occur in MW-mass galaxies; e.g. Roškar et al. 2014). Additionally, momentum imparted by SN feedback can compress existing gas at lower densities, resulting in extended star formation (e.g. Kimm et al. 2015; Jackson et al. 2021b; Martin-Alvarez et al. 2023), which

can dilute the stellar profile further, leading to the formation of low surface brightness systems (e.g. Martin et al. 2019; Jackson et al. 2021b).

NEWHORIZON lacks gentler forms of feedback that can regulate the impact of SNe. In real galaxies, young stellar clusters are surrounded by H II regions, which result from the ionizing radiation those young stars produce. Because this emerges from the photopheres of massive stars, this feedback sets in before SNe. It has a similar impact as SN feedback insofar as it prevents runaway collapse, but it does so without significant mass loading (e.g. Rosdahl & Teyssier 2015; Emerick, Bryan & Mac Low 2018; Agertz et al. 2020). Radiation, and stellar winds, thus can reduce SFRs (e.g. Emerick et al. 2018), resulting in fewer SNe and thus less momentum transfer per unit time.

Of course, NEWHORIZON uses various prescriptions to take such effects into account. For example, the SN rate is enhanced over what is predicted by the chosen IMF, to simulate the influence of gas rarification via the collected influence of clustered SNe (following Kim, Ostriker & Raileanu 2017; Gentry et al. 2019). Additionally, per-SN momentum is increased to take into account the radiative feedback from OB stars, following Geen et al. (2015). While such assumptions are theoretically well motivated, enhancing either the SN rate or the momentum transferred from them likely also serves to enhance the mass loading.

The directionality of feedback can also influence how this momentum is distributed. Real H II regions often show patchy morphology (e.g. Hannon et al. 2019), implying that the corridors through which SN momentum propagates in this way are more constrained (sometimes very much so, e.g. Kim et al. 2023). While such effects may average out in more massive galaxies, these effects may be important in shaping galaxies in the dwarf regime.

In the absence of the environment causing the discrepancies described above, baryonic feedback – likely coupled with resolution effects – is likely to be the primary cause behind the increased diffuseness of the NEWHORIZON dwarfs. However, understanding the precise origins of this diffuseness requires identifying the time-step at which the simulated and observed galaxies begin to diverge in size and surface brightness. This, in turn, requires a comparison of real galaxy structural scaling relations across cosmic time, potentially to very high redshift, which is beyond the scope of this study. High-resolution space-based instruments such as *JWST* (Gardner et al. 2006) should prove useful for making such a comparison in the future.

6 SUMMARY

Using synthetic images and existing derived parameters, we compared dwarf galaxy scaling relations between those found in the two largest groups in the NEWHORIZON simulation with those measured from the FDS. Despite the differences in mass between these groups and Fornax, the latter contains one of the best available catalogues of spatially resolved dwarf galaxy parameters in a dense environment, hence is useful as a comparison. We employed the same techniques to estimate these parameters from NEWHORIZON as were employed in the FDS, thus removing as much methodological uncertainty as possible from the comparison.

While the NEWHORIZON dwarfs have similar Sérsic indices and have a similar fraction containing central light concentrations as their Fornax counterparts, they differ in most other parameters. NEWHORIZON dwarfs are (per unit stellar mass) less luminous, more extended in half-light radius, bluer in colour, and fainter in surface brightness (central and effective) than dwarfs found in the Fornax Cluster. The starkest contrast is in surface brightness, with NEWHORIZON dwarfs being 3–4 mag arcsec^{-2} fainter than their Fornax counterparts. This difference remains even after correcting for the offset in luminosity, implying that the starlight in NEWHORIZON dwarfs is more radially extended than it should be.

Comparison with dwarfs from other observational studies shows that observed dwarfs vary only subtly with the environment in mass–size (half-light radius) and mass–surface brightness relations. Likewise, comparing our results in NEWHORIZON with those of a previous study (Jackson et al. 2021b) shows that the simulation–observation offset is present across all of NEWHORIZON, not just the two largest groups (and appears to be independent of how size is measured from the particle data). Together, this implies that the diffuseness of NEWHORIZON dwarfs is not primarily a result of environment.

Instead, baryonic feedback, likely coupled with resolution effects (particularly at high redshift), seems the more prominent cause. The precise impact of feedback in a simulation is difficult to determine, however, given the aforementioned coupling with resolution, as well as the evolution over time as the gas, stellar, and dark matter mass in any individual galaxy grows through accretion. Without an array of observed dwarf galaxy scaling relations to compare without to high redshift, we cannot determine the precise conditions under which the mass–size offset sets in. Identifying this mechanism using future observations should help refine feedback prescriptions in simulations to come, resulting in more realistic simulated low-mass galaxies.

Ultimately, we have demonstrated that a simulation that reproduces observed integrated galaxy properties may not necessarily reproduce the detailed structures of those same galaxies. These 2D properties can thus provide important additional constraints on feedback prescriptions (including how these interact with the simulation's resolution), which can significantly impact their predictive power. Given their sensitivity to such prescriptions, dwarfs provide an ideal laboratory for the processes that shape the spatial structure of galaxy components, and so the large dwarf samples expected to be observed in and outside the local Universe in large surveys such as *Euclid* (Laureijs et al. 2011) or the Legacy Survey of Space and Time (Ivezić et al. 2019) will help broaden the scope of these comparisons to a wide variety of local conditions and redshifts.

ACKNOWLEDGEMENTS

We thank the anonymous referee for their thorough and helpful report that improved the clarity and quality of this paper. SK and AEW acknowledge support from the Science and Technology Facilities Council (STFC; grant numbers ST/X001318/1 and ST/Y001257/1). SK also acknowledges a Senior Research Fellowship from Worcester College, University of Oxford. GM acknowledges support from the STFC under grant number ST/X000982/1. SKY acknowledges support from the National Research Foundation of Korea (2020R1A2C3003769 and RS-2022-NR070872). This work made use of ASTROPY:[3] a community-developed core PYTHON package and an ecosystem of tools and resources for astronomy (Astropy Collaboration 2013, 2018, 2022). This research made use of PHOTUTILS, an ASTROPY package for detection and photometry of astronomical sources (v.1.11.0; Bradley et al. 2024). This work was granted access to the high performance cluster resources of the Centre Informatique National de l'Enseignement Supérieure (CINES) under the allocations 2013047012, 2014047012, 2015047012, c2016047637,

[3] http://www.astropy.org

A0020407637 made by the Grand Équipement National de Calcul Intensif (GENCI) and KSC-2017-G2-0003 by the Korea Institute of Science and Technology Information (KISTI), and as a 'Grand Challenge' project granted by GENCI on the AMD-Rome extension of the Joliot Curie supercomputer at the Très Grand Centre de Calcul (TGCC), and under the allocation 2019-A0070402192 made by GENCI. This research is part of the Segal (ANR-1919-CE31-0017, http://secular-evolution.org) and Horizon-UK projects. This work has made use of the Infinity cluster on which the simulation was post-processed, hosted by the Institut d'Astrophysique de Paris. We warmly thank S. Rouberol for running it smoothly.

DATA AVAILABILITY

The simulation data analysed in this paper were provided by the NewHorizon Collaboration. The data will be shared on request to the corresponding author, with the permission of the NewHorizon Collaboration, or may be requested from https://new.horizon-simulation.org/data.html. The observational data underlying this article are available at the Centre de Données Astronomique de Strasbourg (CDS), at 10.26093/cds/vizier.36470100 and https://cdsarc.cds.unistra.fr/viz-bin/cat/J/A + A/660/A69, and at the European Southern Observatory Science Archive Facility, at https://archive.eso.org/cms.html. Isophotal radii for FDS galaxies are published as supplementary data by Watkins et al. (2023).

REFERENCES

Agertz O. et al., 2020, MNRAS, 491, 1656
Astropy Collaboration, 2013, A&A, 558, A33
Astropy Collaboration, 2018, AJ, 156, 123
Astropy Collaboration, 2022, ApJ, 935, 167
Beckmann R. S. et al., 2017, MNRAS, 472, 949
Benincasa S. M., Wadsley J., Couchman H. M. P., Keller B. W., 2016, MNRAS, 462, 3053
Bershady M. A., Jangren A., Conselice C. J., 2000, AJ, 119, 2645
Binney J., Tremaine S., 2008, Galactic Dynamics, 2nd edn. Princeton Univ. Press, Princeton, NJ
Blakeslee J. P. et al., 2009, ApJ, 694, 556
Blanton M. R., Lupton R. H., Schlegel D. J., Strauss M. A., Brinkmann J., Fukugita M., Loveday J., 2005, ApJ, 631, 208
Boselli A., Boissier S., Cortese L., Gavazzi G., 2008, ApJ, 674, 742
Boselli A., Fossati M., Sun M., 2022, A&AR, 30, 3
Boylan-Kolchin M., Bullock J. S., Kaplinghat M., 2011, MNRAS, 415, L40
Bradley L. et al., 2024, astropy/photutils: 1.11.0. Zenodo(https://doi.org/10.5281/zenodo.10671725)
Bruzual G., Charlot S., 2003, MNRAS, 344, 1000
Busko I. C., 1996, in Jacoby G. H., Barnes J., eds, ASP Conf. Ser. Vol. 101, Astronomical Data Analysis Software and Systems V. Astron. Soc. Pac., San Francisco, p. 139
Buzzo M. L. et al., 2024, MNRAS, 529, 3210
Capaccioli M. et al., 2015, A&A, 581, A10
Capriotti E. R., Kozminski J. F., 2001, PASP, 113, 677
Carlsten S. G., Greene J. E., Greco J. P., Beaton R. L., Kado-Fong E., 2021, ApJ, 922, 267
Chabrier G., 2003, PASP, 115, 763
Chabrier G., 2005, in Corbelli E., Palla F., Zinnecker H., eds, Astrophysics and Space Science Library Vol. 327, The Initial Mass Function 50 Years Later. Springer, Dordrecht, p. 41
Chamba N., Hayes M. J., LSST Dark Energy Science Collaboration, 2024, A&A, 689, A28
Cole S., 1991, ApJ, 367, 45
Conselice C. J., 2003, ApJS, 147, 1
Crain R. A. et al., 2015, MNRAS, 450, 1937
Daikuhara K., Kodama T., Pérez-Martínez J. M., Shimakawa R., Suzuki T. L., Tadaki K.-i., Koyama Y., Tanaka I., 2024, MNRAS, 531, 2335
Dale J. E., Ngoumou J., Ercolano B., Bonnell I. A., 2014, MNRAS, 442, 694
Davis F. et al., 2022, MNRAS, 511, 4109
Dayal P., Ferrara A., Dunlop J. S., Pacucci F., 2014, MNRAS, 445, 2545
Di Cintio A., Brook C. B., Dutton A. A., Macciò A. V., Obreja A., Dekel A., 2017, MNRAS, 466, L1
Draine B. T. et al., 2007, ApJ, 663, 866
Drinkwater M. J., Gregg M. D., Colless M., 2001, ApJ, 548, L139
Drinkwater M. J., Jones J. B., Gregg M. D., Phillipps S., 2000, Publ. Astron. Soc. Aust., 17, 227
Driver S. P., Phillipps S., Davies J. I., Morgan I., Disney M. J., 1994, MNRAS, 268, 393
Dubois Y. et al., 2014, MNRAS, 444, 1453
Dubois Y. et al., 2021, A&A, 651, A109
Duc P.-A. et al., 2015, MNRAS, 446, 120
Eliche-Moral M. C., Rodríguez-Pérez C., Borlaff A., Querejeta M., Tapia T., 2018, A&A, 617, A113
Ellison S. L., Patton D. R., Simard L., McConnachie A. W., 2008, AJ, 135, 1877
Emerick A., Bryan G. L., Mac Low M.-M., 2018, ApJ, 865, L22
Federrath C., Klessen R. S., 2012, ApJ, 761, 156
Feldmann R. et al., 2023, MNRAS, 522, 3831
Ferguson H. C., Sandage A., 1990, in Hollenbach D. J., Thronson H. A., Jr, eds, NASA Conf. Publ. Vol. 3084, The Interstellar Medium in External Galaxies: Summaries of Contributed Papers. NASA, Washington, DC, p. 281
Gardner J. P. et al., 2006, Space Sci. Rev., 123, 485
Garrison-Kimmel S. et al., 2019, MNRAS, 487, 1380
Geen S., Rosdahl J., Blaizot J., Devriendt J., Slyz A., 2015, MNRAS, 448, 3248
Geha M. et al., 2017, ApJ, 847, 4
Gentry E. S., Krumholz M. R., Madau P., Lupi A., 2019, MNRAS, 483, 3647
Guo Q. et al., 2011, MNRAS, 413, 101
Habas R. et al., 2020, MNRAS, 491, 1901
Hamadouche M. L. et al., 2022, MNRAS, 512, 1262
Hammer F. et al., 2024, MNRAS, 527, 2718
Hannon S. et al., 2019, MNRAS, 490, 4648
Hernquist L., Katz N., 1989, ApJS, 70, 419
Holwerda B. W. et al., 2014, ApJ, 781, 12
Hopkins P. F. et al., 2018, MNRAS, 480, 800
Hopkins P. F., Quataert E., Murray N., 2012, MNRAS, 421, 3522
Huertas-Company M. et al., 2013, MNRAS, 428, 1715
Impey C., Bothun G., Malin D., 1988, ApJ, 330, 634
Iodice E. et al., 2016, ApJ, 820, 42
Ivezić Ž. et al., 2019, ApJ, 873, 111
Jackson R. A. et al., 2021a, MNRAS, 502, 1785
Jackson R. A. et al., 2021b, MNRAS, 502, 4262
Jackson R. A. et al., 2024, MNRAS, 528, 1655
Jang J. K. et al., 2024, ApJ, 969, 59
Janz J., Salo H., Su A. H., Venhola A., 2021, A&A, 647, A80
Jedrzejewski R. I., 1987, MNRAS, 226, 747
Kaviraj S. et al., 2017, MNRAS, 467, 4739
Kaviraj S., Lazar I., Watkins A. E., Laigle C., Martin G., Jackson R. A., 2025, preprint (arXiv:2502.02656)
Keel W. C., Kennicutt R. C. J., Hummel E., van der Hulst J. M., 1985, AJ, 90, 708
Kennicutt R. C. J., 1998, ApJ, 498, 541
Kim C.-G., Ostriker E. C., Raileanu R., 2017, ApJ, 834, 25
Kim K. J. et al., 2023, ApJ, 955, L17
Kim S. Y., Peter A. H. G., Hargis J. R., 2018, Phys. Rev. Lett., 121, 211302
Kimm T., Cen R., 2014, ApJ, 788, 121
Kimm T., Cen R., Devriendt J., Dubois Y., Slyz A., 2015, MNRAS, 451, 2900
Kimm T., Katz H., Haehnelt M., Rosdahl J., Devriendt J., Slyz A., 2017, MNRAS, 466, 4826
Klypin A., Kravtsov A. V., Valenzuela O., Prada F., 1999, ApJ, 522, 82
Kobayashi C., Karakas A. I., Lugaro M., 2020, ApJ, 900, 179

Koch A., Burkert A., Rich R. M., Collins M. L. M., Black C. S., Hilker M., Benson A. J., 2012, ApJ, 755, L13
Komatsu E. et al., 2011, ApJS, 192, 18
Kuijken K. et al., 2002, The Messenger, 110, 15
Lacey C., Silk J., 1991, ApJ, 381, 14
Laureijs R. et al., 2011, preprint (arXiv:1110.3193)
Lazar I., Kaviraj S., Watkins A. E., Martin G., Bichang'a B., Jackson R. A., 2024a, MNRAS, 529, 499
Lazar I., Kaviraj S., Watkins A. E., Martin G., Bichang'a B., Jackson R. A., 2024b, MNRAS, 533, 3771
Li Q., Narayanan D., Davé R., 2019, MNRAS, 490, 1425
Lisker T., Glatt K., Westera P., Grebel E. K., 2006, AJ, 132, 2432
Lucy L. B., 1977, AJ, 82, 1013
Ludlow A. D., Schaye J., Schaller M., Bower R., 2020, MNRAS, 493, 2926
Martin G. et al., 2019, MNRAS, 485, 796
Martin G. et al., 2022, MNRAS, 513, 1459
Martin G., Kaviraj S., Devriendt J. E. G., Dubois Y., Pichon C., 2018, MNRAS, 480, 2266
Martin-Alvarez S., Sijacki D., Haehnelt M. G., Farcy M., Dubois Y., Belokurov V., Rosdahl J., Lopez-Rodriguez E., 2023, MNRAS, 525, 3806
Mastropietro C., Moore B., Mayer L., Debattista V. P., Piffaretti R., Stadel J., 2005, MNRAS, 364, 607
McCarthy I. G., Schaye J., Bird S., Le Brun A. M. C., 2017, MNRAS, 465, 2936
McNaught-Roberts T. et al., 2014, MNRAS, 445, 2125
Méndez-Abreu J., Sánchez-Janssen R., Aguerri J. A. L., Corsini E. M., Zarattini S., 2012, ApJ, 761, L6
Mercado F. J. et al., 2025, preprint (arXiv:2501.04084)
Merritt A., Pillepich A., van Dokkum P., Nelson D., Hernquist L., Marinacci F., Vogelsberger M., 2020, MNRAS, 495, 4570
Mihos J. C., 2004, in Duc P.-A., Braine J., Brinks E., eds, Proc. IAU Symp. 217, Recycling Intergalactic and Interstellar Matter. Astron. Soc. Pac., San Francisco, p. 390
Mihos J. C., Hernquist L., 1994, ApJ, 425, L13
Montero-Dorta A. D., Chaves-Montero J., Artale M. C., Favole G., 2021, MNRAS, 508, 940
Montes M., Trujillo I., Infante-Sainz R., Monelli M., Borlaff A. S., 2021, ApJ, 919, 56
Moore B., Ghigna S., Governato F., Lake G., Quinn T., Stadel J., Tozzi P., 1999, ApJ, 524, L19
Moore B., Lake G., Katz N., 1998, ApJ, 495, 139
Moreno J., Torrey P., Ellison S. L., Patton D. R., Bluck A. F. L., Bansal G., Hernquist L., 2015, MNRAS, 448, 1107
Muñoz-Mateos J. C. et al., 2015, ApJS, 219, 3
Munshi F., Brooks A. M., Christensen C., Applebaum E., Holley-Bockelmann K., Quinn T. R., Wadsley J., 2019, ApJ, 874, 40
Okamura S., Kodaira K., Watanabe M., 1984, ApJ, 280, 7
Oñorbe J., Boylan-Kolchin M., Bullock J. S., Hopkins P. F., Kereš D., Faucher-Giguère C.-A., Quataert E., Murray N., 2015, MNRAS, 454, 2092
Oppenheimer B. D., Davé R., 2006, MNRAS, 373, 1265
Ostriker J. P., Spitzer L. J., Chevalier R. A., 1972, ApJ, 176, L51
Padoan P., Nordlund Å., 2011, ApJ, 730, 40
Paulino-Afonso A. et al., 2019, A&A, 630, A57
Peletier R. et al., 2020, preprint (arXiv:2008.12633)
Peñarrubia J., Navarro J. F., McConnachie A. W., 2008, ApJ, 673, 226
Peng C. Y., Ho L. C., Impey C. D., Rix H.-W., 2002, AJ, 124, 266
Peng C. Y., Ho L. C., Impey C. D., Rix H.-W., 2010, AJ, 139, 2097
Pontzen A., Governato F., 2012, MNRAS, 421, 3464
Poulain M. et al., 2021, MNRAS, 506, 5494
Read J. I., Gilmore G., 2005, MNRAS, 356, 107
Román J., Trujillo I., Montes M., 2020, A&A, 644, A42
Romero-Gómez J., Aguerri J. A. L., Peletier R. F., Mieske S., van de Ven G., Falcón-Barroso J., 2024, MNRAS, 527, 9715
Rosdahl J., Teyssier R., 2015, MNRAS, 449, 4380
Roškar R., Teyssier R., Agertz O., Wetzstein M., Moore B., 2014, MNRAS, 444, 2837
Saintonge A., Masters K. L., Marinoni C., Spekkens K., Giovanelli R., Haynes M. P., 2008, A&A, 478, 57
Salo H. et al., 2015, ApJS, 219, 4
Salpeter E. E., 1955, ApJ, 121, 161
Sandage A., Binggeli B., 1984, AJ, 89, 919
Sawala T. et al., 2016, MNRAS, 457, 1931
Schaye J. et al., 2010, MNRAS, 402, 1536
Schaye J. et al., 2015, MNRAS, 446, 521
Schmidt M., 1959, ApJ, 129, 243
Shen S., Mo H. J., White S. D. M., Blanton M. R., Kauffmann G., Voges W., Brinkmann J., Csabai I., 2003, MNRAS, 343, 978
Sheth K. et al., 2010, PASP, 122, 1397
Springel V. et al., 2005, Nature, 435, 629
Springel V. et al., 2018, MNRAS, 475, 676
Su A. H. et al., 2021, A&A, 647, A100
Szomoru D., Franx M., van Dokkum P. G., 2012, ApJ, 749, 121
Taylor E. N. et al., 2011, MNRAS, 418, 1587
Taylor P., Kobayashi C., 2016, MNRAS, 463, 2465
Teyssier R., 2002, A&A, 385, 337
Toloba E. et al., 2015, ApJ, 799, 172
Toomre A., Toomre J., 1972, ApJ, 178, 623
Trujillo I. et al., 2006, ApJ, 650, 18
Trujillo I. et al., 2021, A&A, 654, A40
Trujillo I., Chamba N., Knapen J. H., 2020, MNRAS, 493, 87
Tully R. B., Fisher J. R., 1977, A&A, 54, 661
van der Wel A. et al., 2014, ApJ, 788, 28
Venhola A. et al., 2018, A&A, 620, A165
Venhola A. et al., 2019, A&A, 625, A143
Venhola A. et al., 2022, A&A, 662, A43
Vogelsberger M. et al., 2014, MNRAS, 444, 1518
Watkins A. E. et al., 2022, A&A, 660, A69
Watkins A. E., Salo H., Kaviraj S., Collins C. A., Knapen J. H., Venhola A., Román J., 2023, MNRAS, 521, 2012
Weaver J. R. et al., 2022, ApJS, 258, 11
Weingartner J. C., Draine B. T., 2001, ApJ, 548, 296
Wetzel A. R., Hopkins P. F., Kim J.-h., Faucher-Giguère C.-A., Kereš D., Quataert E., 2016, ApJ, 827, L23
Wetzel A. R., Tinker J. L., Conroy C., van den Bosch F. C., 2013, MNRAS, 432, 336
White S. D. M., Frenk C. S., 1991, ApJ, 379, 52
White S. D. M., Rees M. J., 1978, MNRAS, 183, 341
Williamson D., Martel H., Romeo A. B., 2016, ApJ, 831, 1
Wright R. J., Somerville R. S., Lagos C. d. P., Schaller M., Davé R., Anglés-Alcázar D., Genel S., 2024, MNRAS, 532, 3417
Yang X., Mo H. J., van den Bosch F. C., 2009, ApJ, 693, 830
Yoachim P. et al., 2016, in Peck A. B., Seaman R. L., Benn C. R., eds, Proc. SPIE Conf. Ser. Vol. 9910, Observatory Operations: Strategies, Processes, and Systems VI. SPIE, Bellingham, p. 99101A
Zaritsky D., Donnerstein R., Karunakaran A., Barbosa C. E., Dey A., Kadowaki J., Spekkens K., Zhang H., 2022, ApJS, 261, 11
Zolotov A. et al., 2012, ApJ, 761, 71

This paper has been typeset from a TEX/LATEX file prepared by the author.